Eur. J. Mech. B/Fluids, **17**, n° 3, 331-355, 1998

Boundary layer over a slotted plate

P. LAPLACE * and É. ARQUIS

ABSTRACT. – In order to investigate the boundary layer over a slotted plate, we first set up a hydrodynamic boundary condition for a parallel flow from a numerical study, performed on a periodic perforated medium at the local scale of the perforations. This boundary condition links the shear stress at the wall and the slip velocity along the plate by a partial slip coefficient. Then, a parametric study is conducted to analyse this partial slip coefficient versus the surface porosity of the plate and the Reynolds number of the flow. Afterwards, we introduce this partial slip boundary condition in the Blasius formalism and express the dynamic boundary layer thickness, the reduced slip velocity and the shear stress at the wall as functions of the slip coefficient, the Reynolds number and the reduced abscissa on the plate. Finally, we compare these latter laws with direct simulation results of the boundary layer flow over a slotted plate, considered as a very thin homogeneous permeable flat wall. © Elsevier, Paris.

1. Introduction

Perforated plates and wire nettings occur in many applications of fluid mechanics (such as perforated wings in order to reduce the turbulence by suction of the boundary layer, filtration or air conditioning). These media are often characterized by their pressure drop coefficient which is mostly determined experimentally. When faced with a tangential flow, a no-slip hypothesis is generally taken. However, this assumption is no longer valid when the perforation density becomes sufficiently large since the adhesion of the fluid to the perforated medium is not complete. In a boundary layer flow, this will have consequences for the displacement thickness.

First of all, working on ideal two-dimensional periodic perforated media placed in a purely tangential flow, we prove numerically that the boundary condition $d\mathbf{V}/dn = \beta\,\mathbf{V}$, introduced by Navier in the 19th century and linking the shear stress at the wall and the slip velocity by the coefficient β, applies to slotted plates. By means of an experimental study, this partial slip boundary condition (called the "Navier condition" hereafter) was revived empirically by Beavers and Joseph (1967) for a fluid–porous medium interface. A theoretical justification for it was given by Saffman (1971). Another validation was proposed by Taylor (1971) and Richardson (1971) who carried out experiments and calculations on an artificial mathematical model of a porous medium.

The Navier condition was also used by Richardson (1973), Hocking (1976) and more recently by Miksis and Davis (1994), Tuck and Kouzoubov (1995) and by Sarkar and Prosperetti (1996) to study tangential viscous fluid flows over periodic or stochastic rough surfaces. Earlier, Laurmann (1961) and Fendell (1970) had worked on the linearization of the equations governing the viscous fluid flow past a flat plate with a slip condition.

In order to prove that the partial slip condition applies to slotted plates, we propose a numerical study of a two-dimensional fluid flow on a slotted plate at a "microscopic scale" (*i.e.* the scale of the perforations which is typically of the order of a millimetre). The influence of geometric parameters (such as the perforation rate and the geometry of the basic cell) and physical properties of the flow (expressed through the Reynolds number) is analysed here.

Laboratoire MASTER–E.N.S.C.P.B., Avenue Pey-Berland, B.P. 108, 33402 Talence Cedex, France
* Correspondence and reprints

0997-7546/98/03/© Elsevier, Paris

Afterwards, we introduce the partial slip boundary condition in the Blasius formalism (and thus obtain a new formalism that we call "a modified Blasius boundary layer problem"). Then we solve the Blasius equation with the new boundary condition using a simple numerical method.

The "macroscopic" (*i.e.* in relation to the whole length of the plate which is typically of the order of a metre) results obtained, show the influence of the dimensionless slip coefficient β_L and of the Reynolds number Re_L, both based on the length L of the plate, the boundary layer thickness, the slip velocity and the shear stress at the wall. We propose some relations which express the evolution of the three previous characteristics of the flow as functions of β_L, Re_L and x/L, the reduced abscissa on the plate. We also quantify these functions for chosen ranges of values of the coefficient β_L.

However, the modified Blasius boundary layer problem introduces some assumptions which are not clearly justified. Therefore, the next stage consists in trying to obtain the same results while solving the complete Navier–Stokes equations with a direct numerical simulation code, in order to compare our "theoretical" laws with the real phenomena that occur over a slotted plate placed in a purely tangential flow. For this purpose, we consider our horizontal slotted plate as a macroscopic, very thin homogeneous permeable boundary for which permeability relative to a length L is expressed by the coefficient β_L.

Thanks to this direct numerical simulation, we can investigate the reduced slip velocity and the shear stress at the wall as functions of β_L, Re_L and the length L of the plate and check the limits of the modified Blasius formalism.

2. Boundary condition for a slotted plate

In 1971, Saffman proposed a theoretical justification for an empirical partial slip boundary condition introduced in 1967 by Beavers and Joseph, for an interface between a fluid and a porous medium. This boundary condition links the shear stress at the wall ($d\mathbf{V}/dn$) and the slip velocity ($\mathbf{V}$) by a coefficient of proportionality (β). It can be used to express the boundary behaviour of total adhesion ($\beta=+\infty$ and therefore $\mathbf{V}=\mathbf{0}$) and of total slip ($\beta=0$ and therefore $d\mathbf{V}/dn=\mathbf{0}$).

We intend to prove numerically that this partial slip boundary condition applies to slotted plates.

The method used here requires the simultaneous study of the problem at the macroscopic scale (the perforated medium is considered as an imaginary homogeneous permeable continuous medium) and also at a microscopic scale (the scale of the perforations).

2.1. Introduction of a theoretical relation between the flow rate and the slip coefficient

Let us consider the one-dimensional macroscopic problem of a parallel viscous fluid flow in the plane of a two-dimensional channel made of a periodic assembly of microscopic basic cells (*see* Figure 1). These cells are made of a succession of very thin horizontal parallel strips of length α, distant from each other by a length γ in the horizontal direction x and by a height $H/2$ in the vertical direction z (*see* Figure 2). The flow is generated by a pressure gradient established in the x-direction between the entry and the exit of the basic cell, whose dimensions are shown in Figure 2.

The established flow of an incompressible viscous fluid in a channel of a total height $H/2$, bounded by two perforated surfaces characterized by a slip coefficient β, is expressed by the reduced Navier–Stokes equation:

$$C+\mu\frac{\partial^2 V_x}{\partial z^2}=0 \quad \text{where} \quad C=-\frac{\partial p}{\partial x}=-\frac{\Delta p}{L} \quad \text{is a constant} \tag{1}$$

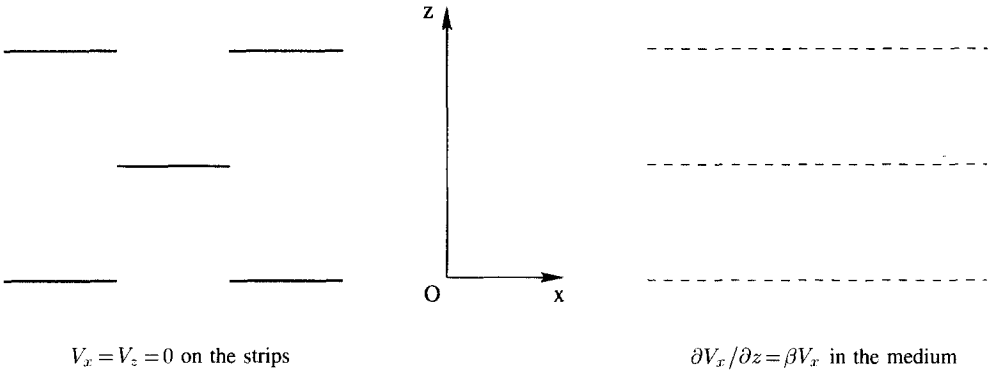

Fig. 1. – Two-dimensional microscopic basic cell (a) constituent of the periodic macroscopic channel (b).

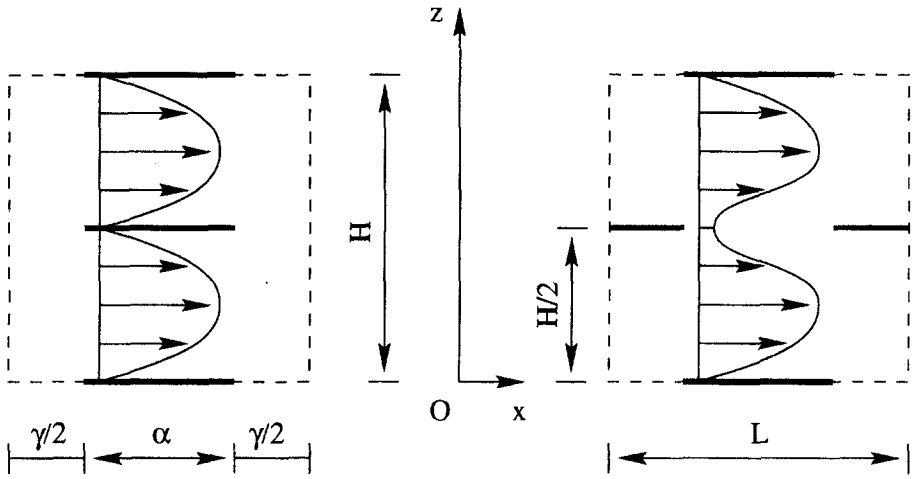

Fig. 2. – Two-dimensional basic cells. Layout of the strips in aligned or staggered rows and representation of the velocity profile.

associated with the boundary conditions:

$$\text{(i)} \quad z = \frac{H}{4}, \quad \frac{\partial V_x}{\partial z} = 0 \quad \text{(by symmetry)} \tag{2}$$

and

$$\text{(ii)} \quad z = 0, \quad \frac{\partial V_x}{\partial z} = \beta V_x \quad \text{(partial slip condition).} \tag{3}$$

The resolution of this trivial system allows the velocity distribution $V_x(z)$ to be explicitly formulated, as well as the flow rate Q in the channel according to the slip coefficient β. We obtain:

$$V_x(z) = -\frac{C}{4\mu}\left[\left(2z^2 - Hz\right) - \frac{H}{\beta}\right] \tag{4}$$

and

$$Q = 2\int_0^{H/2} V_x \, dz = C\frac{H^2}{4\mu}\left(\frac{H}{12} + \frac{1}{\beta}\right). \tag{5}$$

Having chosen L, the extension in the x direction of the basic unit cell, and $\sqrt{(\Delta p/\rho)}$ respectively as length and velocity reference, we can express the reduced (*i.e.* dimensionless) slip coefficient as:

$$\beta_L = \beta L = \frac{A^2}{(Q_H/Re_p) - (A^3/12)} \tag{6}$$

where $A = H/L$ is the aspect ratio of the basic cell, $Re_p = L\sqrt{(\Delta p/\rho)}/\nu$ is the Reynolds number based on the pressure and $Q_H = Q/\left[H\sqrt{(\Delta p/\rho)}\right]$ is the dimensionless flow rate.

2.2. Numerical method for the microscopic problem

Figure 2 represents the two different bi-periodic, two-dimensional media that we will consider in this first study. In the first configuration, the perforations will be laid in aligned rows while they will be placed in staggered rows in the second configuration, in order to quantify the mutual influence of the parallel strips. The thickness of the strips will be the height of the control volumes on which they will be defined.

At first sight, due to the vertical succession of horizontal strips, such a medium does not look like an isolated slotted plate. However, if we progressively increase the height H, the mutual influence of the vertical strips vanishes progressively too and becomes negligible beyond a certain limit. Thus, we can analyse the behaviour of an isolated slotted plate from a study conducted on a finite domain.

By solving the Navier–Stokes equations in the domain presented in Figure 2, we can determine the entire microscopic velocity fields $V_x(x,z)$ and $V_z(x,z)$. A total adhesion boundary condition is adopted for the parallel solid strips. The boundaries are taken to be periodical.

In accordance with a method previously used for the characterization of porous media at a macroscopic scale (Arquis *et al.*, 1991), due to the periodic nature of the medium considered here, we can split up the pressure field $p(x,z)$ into an average field $\bar{p}(x)$ linear in x and a local periodic perturbation $\tilde{p}(x,z)$. Thus, the global pressure field $p(x,z)$ can be written:

$$p(x,z) = \bar{p}(x) + \tilde{p}(x,z) \quad \text{where} \quad \nabla\bar{p}(x) = -\frac{\Delta p}{L} \quad \text{and} \quad \iint \tilde{p}(x,z)\,dx\,dz = 0\,. \tag{7}$$

Here, we are using an iterative procedure to calculate the steady flow. So, the equations of the flow are discretized in time following a first order implicit scheme. Then they are linearized and discretized spatially following the finite volume method on staggered meshes. The coupling between the pressure and the velocity of the flow is processed in primitive variables using the SIMPLER algorithm described in Patankar (1980). The linear systems are solved by a preconditioned conjugate gradient method (BiCGStab–MILU 0) introduced by Van Der Vorst (1992).

In order to determine the refinement of the mesh on which we will perform the computations, we have calculated the value of the reduced slip coefficient β_L as a function of the number of discretization nodes generated on a regular Cartesian two-dimensional mesh. This has been carried out in a domain of surface porosity $\varepsilon_s = 0.50$ consisting of square basic cells of length $H = L = 1$ in which the strips are placed in aligned rows. Table I shows the results obtained, as well as the corresponding computation time required on a server Hewlett–Packard 9000 K200, equipped with four 120 Mhz PA RISC processors and 512 Mb of RAM.

An analysis of Table I reveals that the evolution of the reduced slip coefficient β_L is very moderate beyond $NN = 61^2$ (-1.3 % between $NN = 61^2$ and $NN = 71^2$ then -0.9 % between $NN = 71^2$ and $NN = 81^2$) unlike

TABLE I. – Influence of the number of nodes (NN), generated on a regular Cartesian two-dimensional mesh, on the computation time and the value of the coefficient β_L calculated for the surface porosity $\varepsilon_s = 0.50$ on a domain constituted of square basic cells of length $H = L = 1$, in which the strips are placed in aligned rows.

NN	21^2 = 441	31^2 = 961	41^2 = 1681	51^2 = 2601	61^2 = 3721	71^2 = 5041	81^2 = 6561
computation time (s)	13.5	31	66	120	195	302	443
β_L	28.65	25.76	24.54	23.87	23.44	23.14	22.92

the computation time which dramatically increases. Moreover, the increase of the number of discretization nodes requires that the appropriate amount of RAM be available. Consequently, in order to process all the cases we intend to study, it appears that we can not work with a very fine mesh.

Thus, we will use a Cartesian mesh of 61×61 points for a square domain of length $L = 1$. In order to preserve the same accuracy in every case when changing the aspect ratio, we have decided to increase the number of nodes along the z-axis proportionally to the height H of the basic cell.

2.3. COMPARISON BETWEEN THEORETICAL AND NUMERICAL PROFILES

Now, we have to check *a posteriori* whether it was judicious to suppose the validity of the Navier partial slip condition. To verify this assumption, the procedure is as follows.

For each computation performed at the microscopic scale of the perforations, we calculate the velocity field at each discretization node by resolution of the Navier–Stokes equations and the flow rate in the basic cell. Then, we identify the value of β_L for this flow rate from Equation (6) and insert it into Equation (4) in order to obtain the corresponding macroscopic velocity profile $V_x(z)$. Moreover, from the local velocities obtained by resolution of the microscopic problem, we define the average velocity $\overline{V}_x(z)$ at each ordinate z by the expression:

$$\overline{V}_x(z) = \frac{1}{L} \int_x v_x(x, z)\, dx\,. \tag{8}$$

Then, at each ordinate z, we compare the values taken by $V_x(z)$ and $\overline{V}_x(z)$. If the difference between them is negligible, we will consider that the partial slip condition applies to two-dimensional perforated media.

For every case dealt with here, we notice that the values of $V_x(z)$ and $\overline{V}_x(z)$ are very close, the absolute difference being of the order of 10^{-5} to 10^{-4} and the relative difference of the order of 10^{-6} to 10^{-2} while the velocities are of the order of 10^{-3} to 1. The biggest relative differences are obtained at ordinates where the velocity $V_x(z)$ is very low, thus near the strips.

An increase of Reynolds number or of the height of the basic cell does not increase the difference between $V_x(z)$ and $\overline{V}_x(z)$. Only a decrease of the surface porosity $\varepsilon_s = \gamma/L$ appears to be a legitimate source of moderate differences as well as the type of arrangement of the strips. However, except on (and sometimes very near) the strips in some cases, these relative differences remain definitely lower than 1%.

This verification *a posteriori* allows us to conclude that the Navier condition applies in a very satisfactory way to the study of a viscous fluid flow over a slotted plate modelled by an ideal two-dimensional system, and therefore to justify the identification of the parameter β_L by the relation (6).

2.4. Parametric study

Now that the use of the partial slip boundary condition is justified within the context that interests us, we propose to analyse the evolution of the slip coefficient according to the different parameters of the problem.

2.4.1. *Influence of the type of strip arrangement*

Let us recall that, in this study, we have considered two types of arrangement of the perforations (or the strips) in order to quantify the mutual influence of the parallel strips (*see* Figure 2).

As shown in Table II, in the case of a square basic cell of edge $H=L=1$ (so for an interplate distance $H/2=0.5$), the type of arrangement of the perforations has a noticeable influence on the value of the coefficient β_L. Whatever the surface porosity ε_s and the Reynolds number Re_L, this coefficient β_L is always greater when calculated for a layout in aligned rows than in staggered rows. This point appears to be logical, since the strips are closer to each other at constant abscissa in the arrangement in aligned rows than in staggered rows. In addition, the relative difference between the two types of layout increases as the surface porosity ε_s increases.

Table II. – Coefficient β_L as a function of the interplate distance $H/2$ for different surface porosities ε_s and two types of strip arrangement.

β_L	$\varepsilon_s = 0.20$		$\varepsilon_s = 0.50$		$\varepsilon_s = 0.80$	
$H/2$	Strips in aligned rows	Strips in staggered rows	Strips in aligned rows	Strips in staggered rows	Strips in aligned rows	Strips in staggered rows
0.5	162.413	152.630	23.433	17.862	6.828	5.171
1.0	155.077	154.132	20.073	19.520	5.851	5.687
1.5	155.226	155.035	19.823	19.786	5.782	5.782

2.4.2. *Search for an asymptotic value*

Due to the closed domain chosen for the calculations, the slip coefficient that we determine refers to superimposed slotted plates under mutual influence. In order to find an intrinsic slip coefficient, we have to check that β_L tends towards an asymptotic value when the height H of the basic cell tends towards $+\infty$.

This does not contradict the definition of the coefficient β_L given by Equation (6) insofar as, at fixed pressure gradient Δp and then at constant Reynolds number Re_p, the reduced flow rate Q_H increases when the height H increases. Therefore, β_L does not tend towards 0 when H tends towards $+\infty$.

At constant surface porosity ε_s, whatever the strip arrangement is, the numerical results show that the coefficient β_L tends quickly towards the same asymptotic value as the height $H/2$ between two consecutive vertical strips increases (*see* Table II). The convergence is reached from above for an arrangement in aligned rows and from below for an arrangement in staggered rows.

It is very interesting to discover that we can find a value characterizing a nearly isolated plate from a study conducted in a finite domain. Obviously, it is this asymptotic value that should be used to study the development of a boundary layer over a single slotted or perforated plate.

The results that we will discuss hereafter correspond to the evolution of the asymptotic value of β_L with the Reynolds number Re_L and the surface porosity ε_s. In practice, these asymptotic values have been obtained from calculations carried out on a periodic perforated medium made of strips laid in aligned rows, in which

the height of the basic cell is $H=4$ and therefore on a Cartesian mesh of 61×241 discretization nodes. We have chosen this type of strip arrangement since the convergence of the computations appeared to be much faster with this layout than with staggered rows.

2.4.3. *Influence of the Reynolds number*

Due to the periodicity of the medium, the control parameter of the flow is Re_p, the Reynolds number based on the pressure imposed between the entry and the exit of the basic cell. However, it is easy to express it in terms of velocity which is more convenient and usual. Thus, let us define the Reynolds number Re_L based on the velocity of the flow by the relation:

$$Re_L = Q_H\, Re_p \tag{9}$$

where Q_H is the dimensionless flow rate previously introduced in Section 2.1.

Its influence on the coefficient β_L is interesting to analyse (*see* Figure 3). Indeed, we notice that this coefficient remains constant for the low values of Re_L while it increases regularly beyond $Re_L \approx 10$. Furthermore, the value of Re_L beyond which β_L increases appears to depend on the surface porosity: it increases as ε_s decreases.

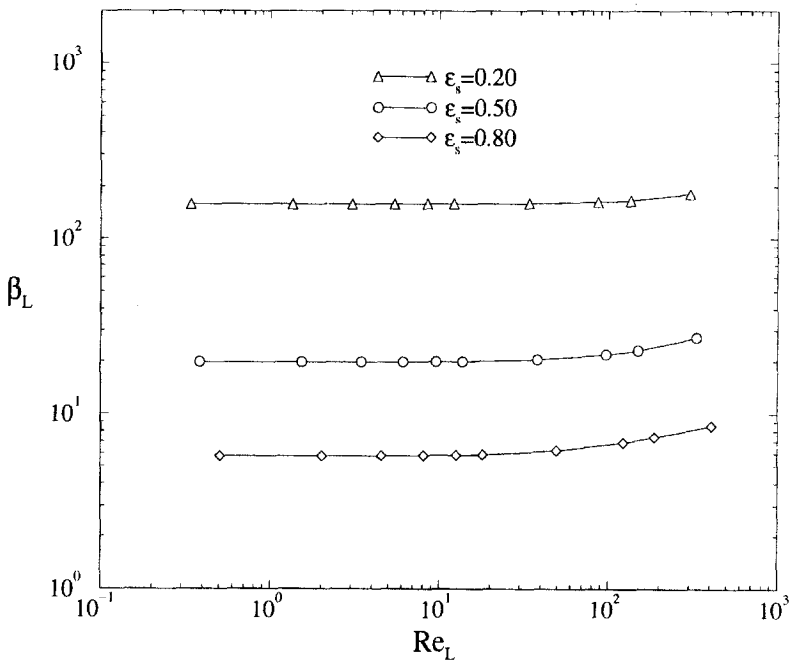

Fig. 3. – Asymptotic value of the coefficient β_L as a function of the Reynolds number Re_L for different surface porosities ε_s.

In practice, our results show that for high flow velocities, a slotted plate, even of quite high surface porosity, behaves rather like a continuous one.

2.4.4. *Influence of the surface porosity*

It appears that the coefficient β_L decreases when the surface porosity ε_s of the medium increases whatever the Reynolds number is. Figure 4 shows this property for different Reynolds numbers $Re_L < 10$ calculated

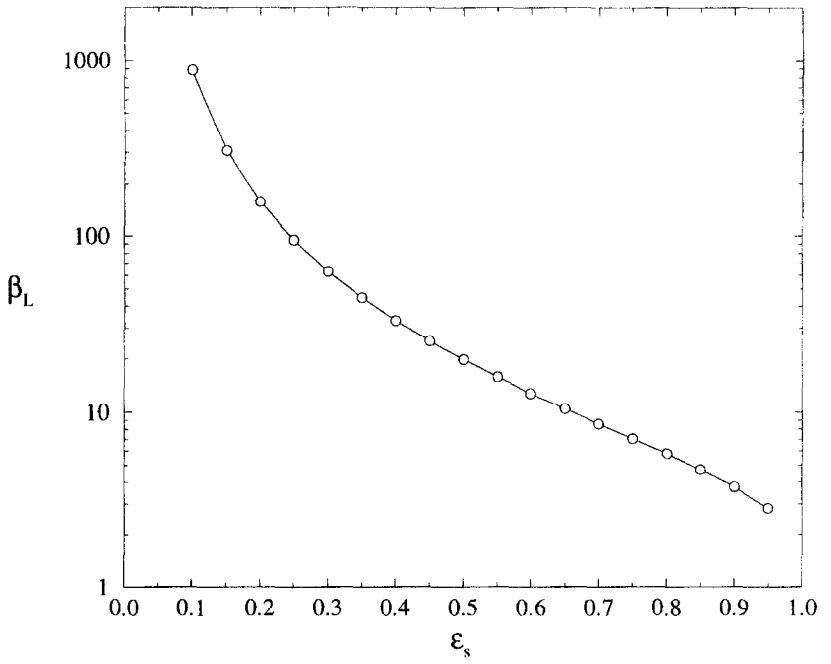

Fig. 4. – Asymptotic value of the coefficient β_L as a function of the surface porosity ε_s for different Reynolds numbers $Re_L < 10$.

from Equation (9) with the single value $Re_p = 1$. Let us recall that the coefficient β_L is independent of those low Reynolds numbers.

The results show that the function $\beta_L = f(\varepsilon_s)$ is of the form:

$$\beta_L = a\,\varepsilon_s^b \quad \text{(with} \quad a \approx 4.2 \quad \text{and} \quad b \approx -2.25\text{)} \quad \text{for} \quad 0.20 \leqslant \varepsilon_s \leqslant 0.50 \tag{10}$$

and of the form:

$$\beta_L = a\,e^{b\varepsilon_s} \quad \text{(with} \quad a \simeq 136.9 \quad \text{and} \quad b \simeq -3.95\text{)} \quad \text{for} \quad 0.60 \leqslant \varepsilon_s \leqslant 0.80\,. \tag{11}$$

Moreover, we notice that β_L tends towards $+\infty$ when ε_s tends towards 0. Then, we find the boundary condition of total adhesion characterizing the viscous fluid flow over a continuous plate. We also approach the boundary condition of total slip quite well which leads to a uniform flow in the absence of plate since β_L seems to tend towards 0 when ε_s tends towards 1.

3. A modified Blasius boundary layer problem

The validity of the Navier condition having been established, we will now examine a modified version of the classical Blasius problem in which the continuous plate is replaced by a homogeneous permeable one. The thickness will remain equal to zero.

So, let us consider the uniform two-dimensional incompressible laminar flow of a Newtonian fluid of constant viscosity and constant velocity U_∞ along the horizontal axis x on a slotted plate (*see* Figure 5). The case of the slotted plate being an extension of that of the continuous plate where just the boundary conditions differ, the equations that govern the boundary layer flow over both a slotted plate on a macroscopic scale and a continuous plate are identical. Furthermore, the simplifying assumptions made in the case of the continuous plate, namely

that the transverse development (characterized by the boundary layer thickness δ) is small, compared with the longitudinal development (characterized by the length L of the plate) and that the forces of viscosity are of the same order as thoses of inertia (Schlichting, 1987), remain rightly valid in the case of the slotted plate. Thus, we suggest that the succession of adherent and non-adherent sections generates only moderate fluctuations of the vertical velocity and therefore of the boundary layer (*see* Figure 5). This hypothesis is consistent with the assumption of zero thickness for the plate which is not very easy to ensure in practice.

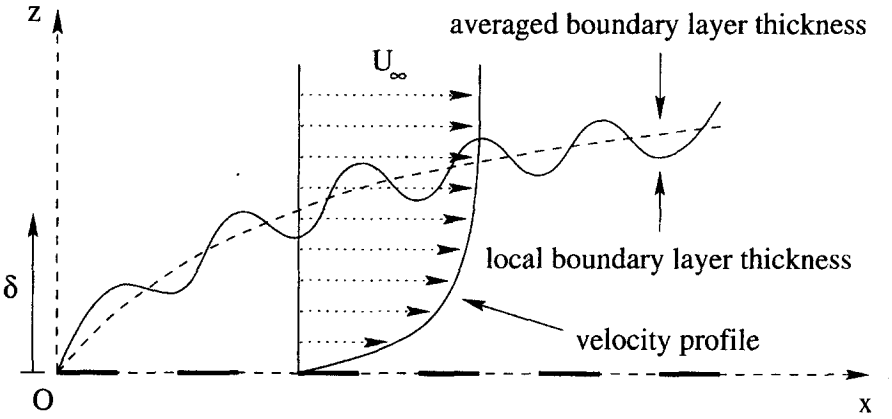

Fig. 5. – Local and averaged boundary layers and velocity profile over a slotted plate.

3.1. Formulation of the governing equations

The problem that we are studying here is described by the same equations as those relative to the case of the continuous plate, that is to say:

$$\frac{\partial V_x}{\partial x} + \frac{\partial V_z}{\partial z} = 0 \qquad \text{(equation of continuity)} \tag{12}$$

and

$$V_x \frac{\partial V_x}{\partial x} + V_z \frac{\partial V_x}{\partial z} = \nu \frac{\partial^2 V_x}{\partial z^2} \qquad \text{(momentum equation)} \tag{13}$$

associated with the boundary conditions:

$$\text{(i)} \quad \left.\frac{\partial V_x(x,z)}{\partial z}\right|_{z=0} = \beta V_x(x,z)\big|_{z=0} \quad \text{(partial slip condition),} \tag{14}$$

$$\text{(ii)} \quad V_z(x,z)\big|_{z=0} = 0 \quad \text{(symmetry of the flow in the plane of the plate)} \tag{15}$$

and

$$\text{(iii)} \quad V_x(x,z)\big|_{z\to+\infty} = U_\infty \quad \text{(linking with the flow at infinity).} \tag{16}$$

Let $F(x,\eta)$ be the dimensionless stream function depending on both the abscissa x on the plate and on the reduced similarity variable $\eta = z\sqrt{(U_\infty/\nu x)} = (z/x)\sqrt{Re_x}$ so that $V_x(x,z)/U_\infty = \partial F(x,\eta)/\partial\eta$.

The introduction of the function $F(x,\eta)$ into the equations of motion (12) and (13) allows these partial derivative equations to be reduced to the single ordinary differential equation for the function $F(x,\eta)$:

$$2\frac{\partial^3 F}{\partial \eta^3} + F\frac{\partial^2 F}{\partial \eta^2} = 0 \qquad \text{(Blasius equation).} \tag{17}$$

The boundary conditions (14), (15) and (16) become, in terms of the function $F(x,\eta)$ and its derivatives:

$$\text{(i)} \quad \left.\frac{\partial^2 F(x,\eta)}{\partial \eta^2}\right|_{\eta=0} = \beta L \sqrt{\frac{\nu}{U_\infty L}}\sqrt{\frac{x}{L}}\left.\frac{\partial F(x,\eta)}{\partial \eta}\right|_{\eta=0} = \beta_L \sqrt{\frac{(x/L)}{Re_L}}\left.\frac{\partial F(x,\eta)}{\partial \eta}\right|_{\eta=0}, \tag{18}$$

$$\text{(ii)} \quad F(x,\eta)\big|_{\eta=0} = 0 \tag{19}$$

and

$$\text{(iii)} \quad \left.\frac{\partial F(x,\eta)}{\partial \eta}\right|_{\eta\to+\infty} = 1\,. \tag{20}$$

We have written the boundary condition (18) in order to bring to the fore the two dimensionless numbers, characteristic of the problem, *i.e.* the reduced slip coefficient $\beta_L = \beta L$ and the Reynolds number $Re_L = U_\infty L/\nu$. However, we notice that — these dimensionless parameters being fixed — the square root of the reduced abscissa x/L appears in this condition. This dependence on the variable x prevents one *a priori* from obtaining similarity of the velocity profiles as with the continuous plate.

3.2. Numerical method for the macroscopic problem

Equation (17) has no analytical solution. But it can be solved numerically in accordance with different methods. Among these, there is one based on series expansions of the functions of the different parameters involved in the problem, and also another one called the "shooting method". This old and classic method is described in several books, for instance in Shih (1984).

The method we propose here consists of replacing the third order differential Blasius equation (17) of the function $F(x,\eta)$ by the two following coupled equations, respectively of the first and second order, of the two functions $F(x,\eta)$ and $G(x,\eta)$:

$$G(x,\eta) = \frac{\partial F(x,\eta)}{\partial \eta} \tag{21}$$

and

$$2\frac{\partial^2 G}{\partial \eta^2} + F\frac{\partial G}{\partial \eta} = 0 \tag{22}$$

associated with the boundary conditions:

$$\text{(i)} \quad \left.\frac{\partial G(x,\eta)}{\partial \eta}\right|_{\eta=0} = \beta_L \sqrt{\frac{(x/L)}{Re_L}}\, G(x,\eta)\big|_{\eta=0}, \tag{23}$$

(24) $$\text{(ii)} \quad F(x,\eta)\big|_{\eta=0} = 0$$

and

(25) $$\text{(iii)} \quad G(x,\eta)\big|_{\eta\to+\infty} = 1\,.$$

In practice, it appears that the boundary condition (25) is already well satisfied for $\eta=10$ in the range of Reynolds numbers studied here.

Equations (21) and (22) are first discretized following a finite difference method on staggered meshes for the variables $F(x,\eta)$ and $G(x,\eta)$.

Equation (21) is solved very simply by the explicit scheme:

(26) $$F_{i+1} = F_i + \Delta\eta\, G_i\,, \quad i>0\,,$$

while Equation (22) is first put into the conservative form:

(27) $$2\,G'' + \left[(FG)' - F'G\right] = 0$$

before being processed in a pseudo-unsteady form by a first order implicit scheme of the Gauss–Seidel kind (for instance).

The resolution of these equations has been performed on a fine mesh of 201 points representing a range of η varying from 0 to 10.

We will see later that our method provides very accurate results.

3.3. Parametric study

Considering the dependence of the slip coefficient β_L on the Reynolds number Re_L beyond a certain threshold (*see* Section 2.4), we have limited our study to sufficiently low values of Re_L so that they do not influence the value of β_L. This is compatible with the assumption we have made, that we are working with a laminar flow. On the other hand, we will sometimes find low values (*i.e.* of 10) of the Reynolds number. The use of these low values could seem inconsistent with the boundary layer hypotheses that we have made but it is not: according to the relations (18) or (23), we are not studying here the influence of the single Reynolds number but the influence of the ratio $\beta_L/\sqrt{Re_L}$ on the main characteristics of the boundary layer flow. Actually, the ratio obtained with $Re_L = 100$ and $\beta_L = 10$ is identical to the one obtained with $Re_L = 10^4$ and $\beta_L = 100$.

3.3.1. *Evolution of the reduced horizontal velocity for different values of the reduced slip coefficient*

Figure 6 shows the evolution of the function $G(x,\eta)$, which is nothing else than the reduced horizontal velocity $V_x(x,z)/U_\infty$, for different values of the coefficient β_L and for x/L and Re_L fixed respectively at 1 and 100.

First, we verify that we find the classical results of the Blasius problem when the coefficient β_L tends towards $+\infty$. As a matter of fact, the horizontal velocity is equal to zero at the wall and it reaches U_∞ for $\eta=4.91$. We remind the reader that this case corresponds to the one of the continuous plate.

We notice that the influence of the coefficient β_L on $G(x,\eta)$ is poor beyond $\beta_L=100$ and becomes almost non-existent beyond $\beta_L=1,000$ (at $Re_L=100$). So, for these flow conditions, a slotted plate behaves nearly like a continuous plate.

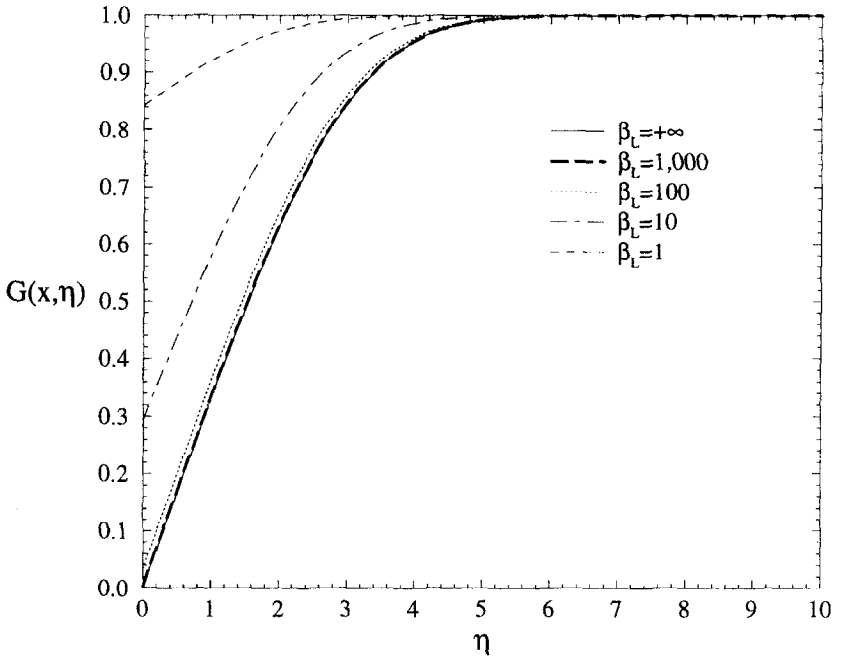

Fig. 6. – Horizontal reduced velocity $G(x,\eta) = V_x(x/L,z)/U_\infty$ for different values of the coefficient β_L, $x/L=1$ and $Re_L=100$.

On the other hand, below $\beta_L = 100$ (still for $Re_L = 100$), a slotted plate cannot be considered as a continuous plate since the adhesion of the fluid at the wall is no longer complete. Moreover, we confirm that we do tend towards the borderline case of total slip when β_L becomes low.

In short, due to the dependence of the coefficient β_L on the Reynolds number of the flow Re_L, our results prove that we can consider as continuous every slotted plate whose reduced slip coefficient β_L is greater than $10\sqrt{Re_L}$.

3.3.2. *Boundary layer thickness and reduced slip velocity*

As a result of the dimensional analysis, we can write *a priori* the boundary layer thickness δ (which is arbitrarily taken equal to 99 % of U_∞) and the reduced slip velocity on the plate V_p as functions of the space and flow parameters, that is to say:

$$\frac{\delta}{L} = A\left(\beta_L, \frac{x}{L}, Re_L\right)\sqrt{\frac{(x/L)}{Re_L}} \tag{28}$$

and

$$V_p = \left.\frac{V_x(x,z)}{U_\infty}\right|_{z=0} = B\left(\beta_L, \frac{x}{L}, Re_L\right)\sqrt{\frac{Re_L}{(x/L)}}\,. \tag{29}$$

The functions A and B introduced in Equations (28) and (29) depend *a priori* on the reduced slip coefficient β_L, on the reduced abscissa x/L and on the Reynolds number of the flow Re_L.

In order to quantify these two functions, we show their dependence on to the single parameter β_L for two positions x/L and three values of Re_L for a total of four different ratios $[(x/L)/Re_L]$ (*see* Figures 7 and 8).

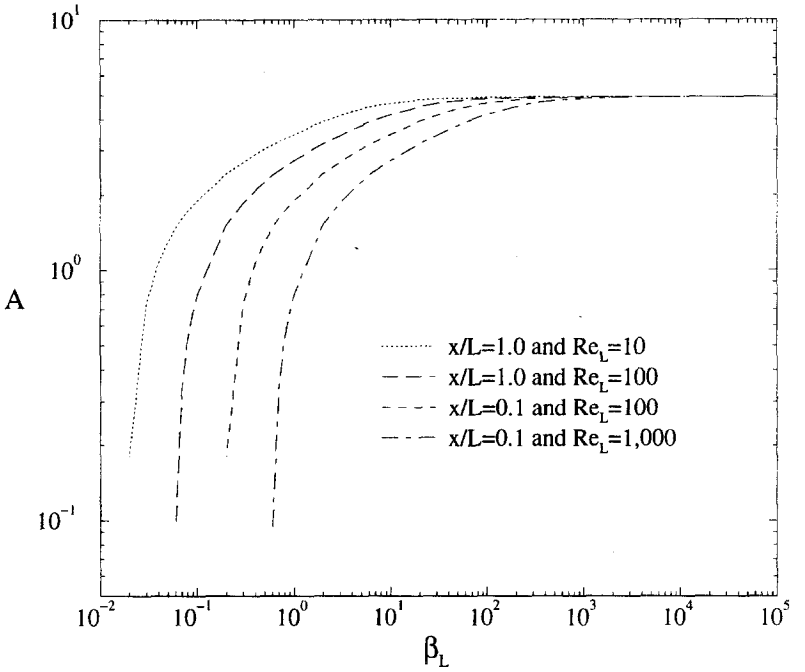

Fig. 7. – Evolution of the function $A(\beta_L, x/L, Re_L)$.

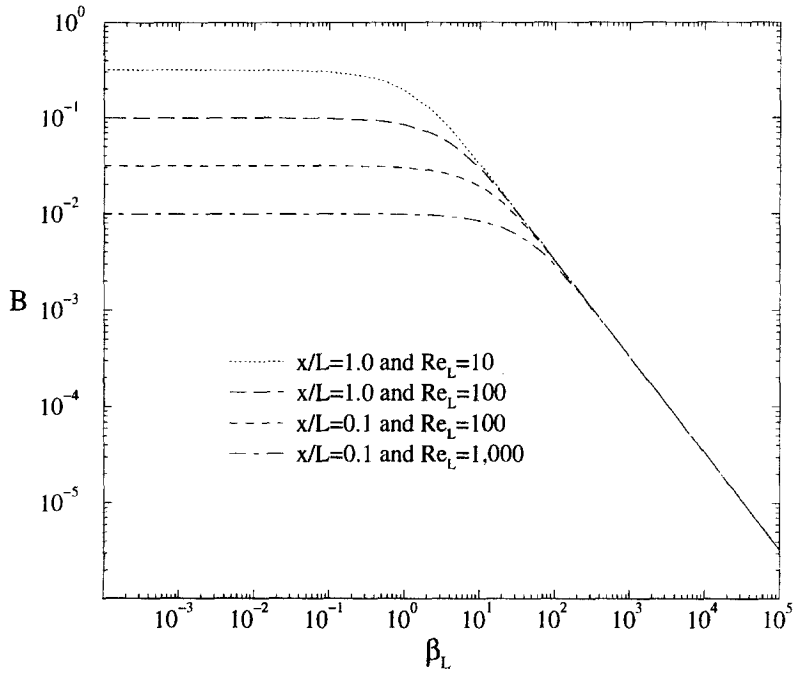

Fig. 8. – Evolution of the function $B(\beta_L, x/L, Re_L)$.

First, we notice that, on both figures, the different curves present exactly the same behaviour. We can infer any function A or B for any pair $[(x/L), Re_L]$ from a single curve of reference obtained for $[(x/L)/Re_L]=1$ by a translation which depends on $\sqrt{(x/L)/Re_L}$.

Indeed, we have:

$$A\left(\beta_L, \frac{x}{L}, Re_L\right)\Big|_{[(x/L)/Re_L]=1} = A\left[\beta_L \sqrt{\frac{(x/L)}{Re_L}}, \frac{x}{L}, Re_L\right]\Bigg|_{[(x/L)/Re_L]} \tag{30}$$

and

$$B\left(\beta_L, \frac{x}{L}, Re_L\right)\Big|_{[(x/L)/Re_L]=1} = \sqrt{\frac{Re_L}{(x/L)}}\, B\left[\beta_L \sqrt{\frac{(x/L)}{Re_L}}, \frac{x}{L}, Re_L\right]\Bigg|_{[(x/L)/Re_L]} . \tag{31}$$

Function A displays an asymptotic behaviour for high values of β_L. The result obtained shows that the boundary layer thickness varies exactly like one which developing on a continuous plate, a result that was not taken for granted *a priori*. So, we propose the expression:

$$\frac{\delta}{L} \simeq 4.9 \sqrt{\frac{(x/L)}{Re_L}} \quad \text{for} \quad \beta_L > 100 \sqrt{\frac{Re_L}{(x/L)}} . \tag{32}$$

Concerning the function B, we can see that a main curve of equation $0.332/\beta_L$ groups the different points together for high values of β_L. Thus, for the reduced slip velocity on the plate, we propose the expression:

$$V_p = \frac{V_x(x,z)}{U_\infty}\bigg|_{z=0} = \frac{0.332}{\beta_L} \sqrt{\frac{Re_L}{(x/L)}} \quad \text{for} \quad \beta_L \geqslant 40 \sqrt{\frac{Re_L}{(x/L)}} . \tag{33}$$

A different asymptotic behaviour stands out for this function for low values of β_L: the function B becomes independent of β_L as this coefficient decreases. It is of the form:

$$B = \sqrt{\frac{(x/L)}{Re_L}} \quad \text{for} \quad \beta_L \leqslant 10^{-3} \sqrt{\frac{Re_L}{(x/L)}} \tag{34}$$

which obviously leads to:

$$V_p = 1 \quad \text{for} \quad \beta_L \leqslant 10^{-3} \sqrt{\frac{Re_L}{(x/L)}} . \tag{35}$$

Speaking more qualitatively, it is interesting to observe the behaviour of the boundary layer thickness and of the reduced slip velocity on the plate, according to the reduced abscissa x/L for different values of the Reynolds number Re_L and of the reduced slip coefficient β_L. In accordance with Equations (28) and (29), we verify that, for a given value of β_L, an increase of Reynolds number causes a decrease of the boundary layer thickness (*see* Figure 9) and, correspondingly, an increase of the reduced slip velocity (*see* Figure 10). It is advisable to note that all the curves on Figure 10 tend to be linked with $V_p=1$ at $x=0$ due to the boundary

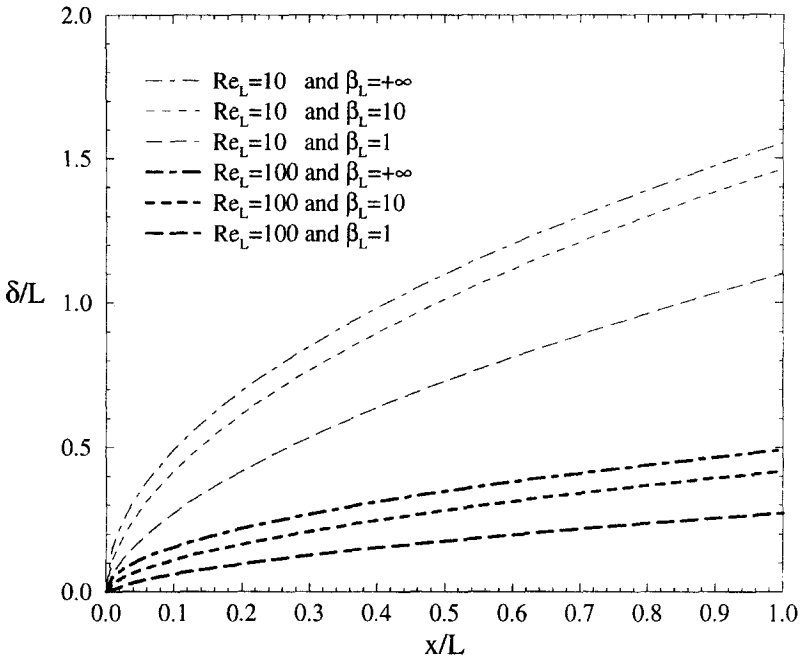

Fig. 9. – Reduced boundary layer thickness δ/L as a function of x/L for different values of the Reynolds number Re_L and of the coefficient β_L.

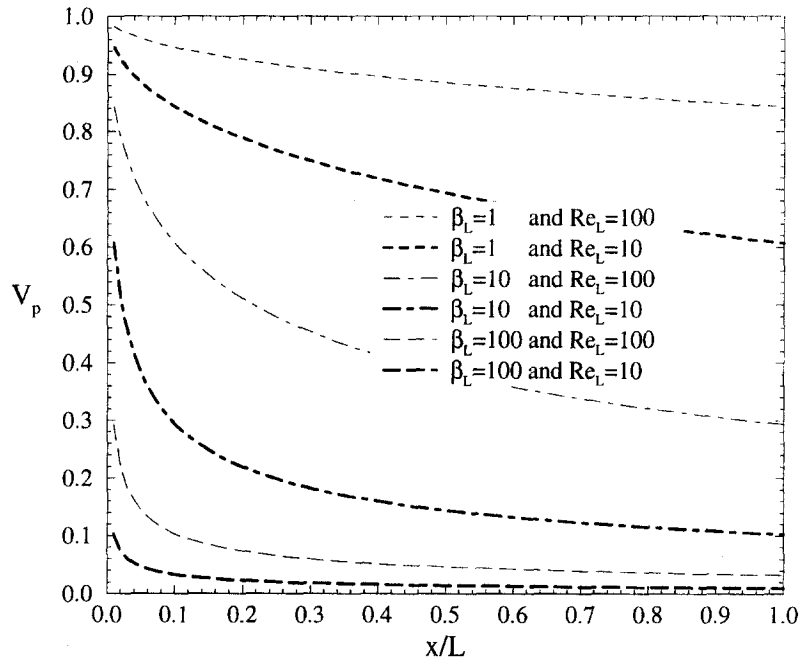

Fig. 10. – Reduced slip velocity on the plate $V_p = [V_x(x,z)/U_\infty]_{z=0}$ as a function of x/L for different values of the coefficient β_L and of the Reynolds number Re_L.

conditions $V_x(x,z)|_{x=0} = U_\infty$ and $V_z(x,z)|_{x=0} = 0$ imposed at the entry of the computation domain, although this point is singular and therefore cannot be calculated.

For high values of the reduced slip coefficient β_L, the reduced slip velocity tends rapidly towards 0 as we move away from the leading edge of the plate while, for lower values of β_L, the leading edge slip velocity decreases only slightly over a large distance measured from the leading edge of the plate.

3.3.3. *Reduced shear stress at the wall*

As we have done for the boundary layer thickness and the reduced slip velocity, we can write the reduced shear stress at the wall $\tau_w = \partial V_x/\partial z$ as a function of the space and flow parameters, that is to say:

$$\tau_w = C\left(\beta_L, \frac{x}{L}, Re_L\right)\sqrt{\frac{Re_L}{(x/L)}} \tag{36}$$

where C is a function which depends *a priori* on the reduced slip coefficient β_L, on the reduced abscissa x/L, and on the Reynolds number of the flow Re_L.

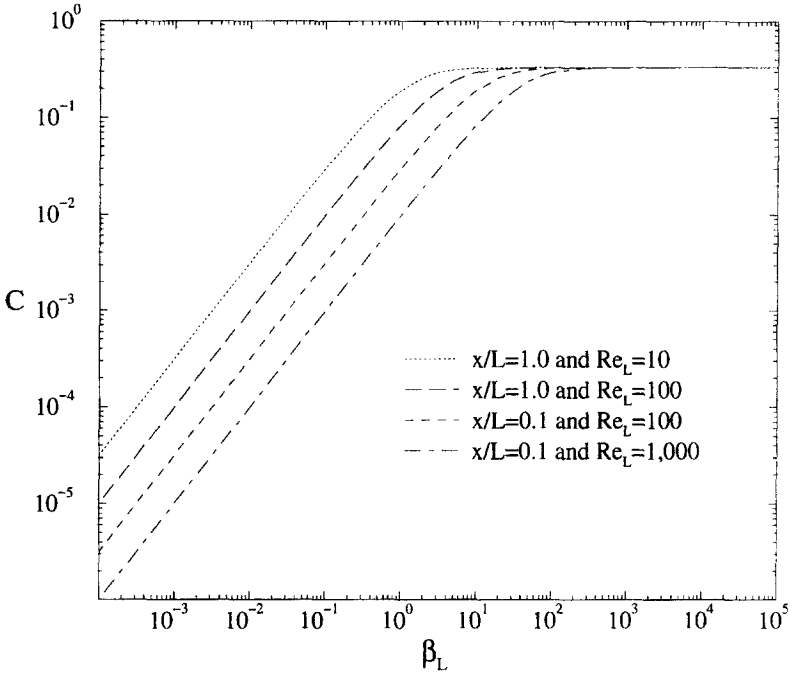

Fig. 11. – Evolution of the function $C(\beta_L, x/L, Re_L)$.

Again, we notice that we can infer any function C for any pair $[(x/L), Re_L]$ from a single curve of reference obtained for $[(x/L)/Re_L]=1$ by a translation which depends on $\sqrt{(x/L)/Re_L}$.

Indeed, we have:

$$C\left(\beta_L, \frac{x}{L}, Re_L\right)\Big|_{[(x/L)/Re_L]=1} = C\left[\beta_L\sqrt{\frac{(x/L)}{Re_L}}, \frac{x}{L}, Re_L\right]\Bigg|_{[(x/L)/Re_L]} \tag{37}$$

Function C presents the same two asymptotic forms of behaviour as function B, introduced in Equation (29). For the reduced shear stress at the wall, we can propose the expressions:

$$\tau_w = 0.332\sqrt{\frac{Re_L}{(x/L)}} \quad \text{for} \quad \beta_L \geqslant 40\sqrt{\frac{Re_L}{(x/L)}} \tag{38}$$

and

$$\tau_w = \beta_L \quad \text{for} \quad \beta_L \leqslant 10^{-3}\sqrt{\frac{Re_L}{(x/L)}}\,. \tag{39}$$

These results totally agree with those obtained for the reduced slip velocity, since they confirm the validity of the partial slip boundary condition. Indeed, we have:

$$C\Big(\beta_L, \frac{x}{L}, Re_L\Big) = \beta_L\, B\Big(\beta_L, \frac{x}{L}, Re_L\Big) \tag{40}$$

and then

$$\tau_w = \frac{\partial V_p}{\partial z} = \beta_L\, V_p \tag{41}$$

which is nothing else than the Navier condition that we have used in this study.

Figure 12 shows the evolution of the reduced shear stress at the wall τ_w according to the reduced abscissa x/L for different values of the Reynolds number Re_L and of the reduced slip coefficient β_L. In accordance with Equations (36) we verify that, for a given value of β_L, an increase in the Reynolds number (respectively in the reduced abscissa x/L) causes an increase (respectively a decrease) in the shear stress at the wall. However, these influences vanish when β_L becomes small, all the more quickly since the Reynolds number is high. Then, the reduced shear stress at the wall becomes constant along the whole length of the plate.

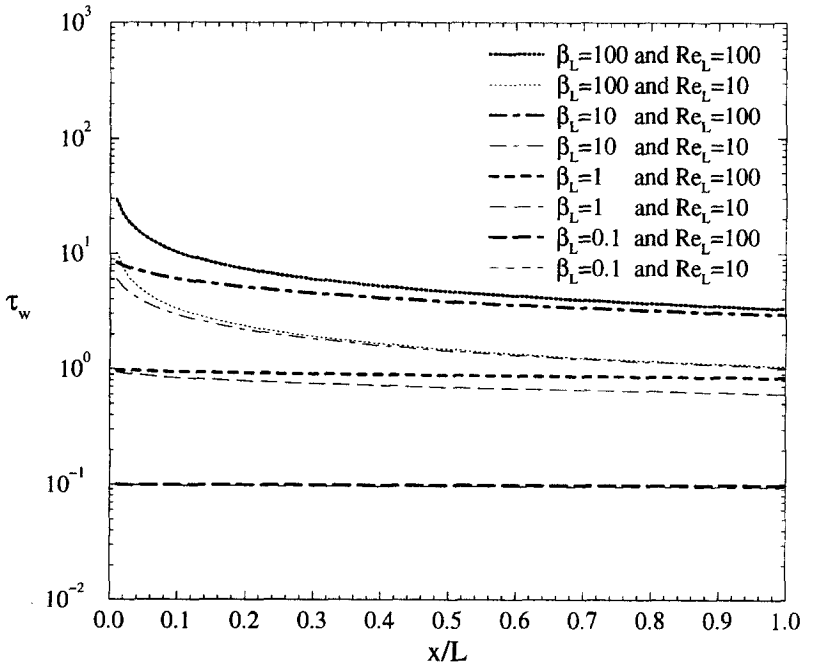

Fig. 12. – Reduced shear stress at the wall τ_w as a function of x/L for different values of the coefficient β_L and of the Reynolds number Re_L.

3.3.4. *Supplementary remarks*

The various asymptotic behaviours that we have indicated clearly include the particular cases of the flow on a continuous flat plate and of the free flow without any solid wall.

Lastly, the opposing roles played by the coefficient β_L and (the square root of) the Reynolds number Re_L that we point out in this study through the relations (18) or (23) are to be expected since the inertia of the flow tends to maintain the velocity at its upstream value while the partial adherence tends, on the contrary, to decelerate the flow.

4. Direct simulation results

So far, we have conducted a study from the boundary layer equations which are simplified Navier–Stokes equations. Consequently, we have considered that the Blasius simplifying boundary layer assumptions could be made in order to study the boundary layer flow over a slotted flat plate considered as a homogeneous permeable flat plate. And we have proved that the main characteristics of a flow over a slotted plate (*i.e.* the boundary layer thickness, the slip velocity and the shear stress at the wall) did depend upon the abscissa x. So, now, we want to check the importance of such a dependence with the use of direct numerical simulations and study whether it could be neglected.

4.1. Modelling of the problem

As shown on Figure 13, we have modelled a computation domain of length L and height H. The height H will remain constant and equal to 1 throughout the study while the length L will vary, as well as the length of the plate. Thus, in order to define and work with the same dimensionless parameters whatever the length of the plate is, we will choose a unit length $l=1$ on the plates as reference length. These parameters will be the reduced slip coefficient β_l and the Reynolds number of the flow Re_l.

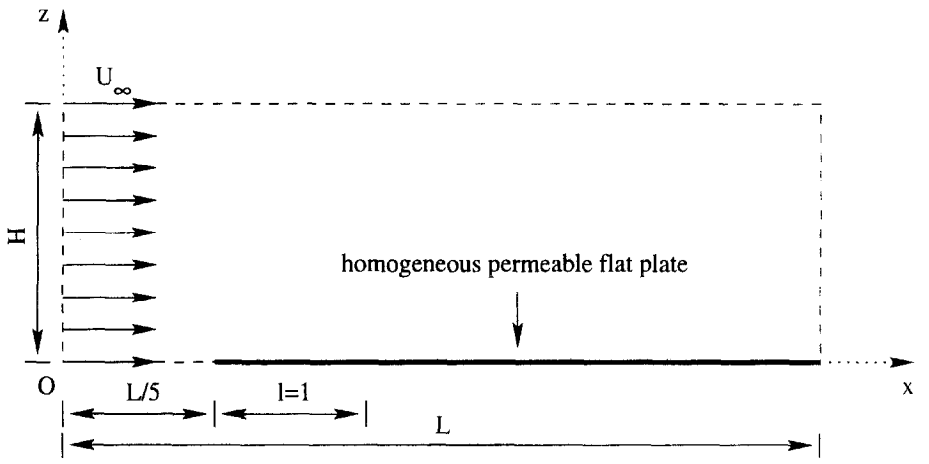

Fig. 13. – Direct numerical simulation—computational domain.

A purely tangential fluid flow of modulus U_∞ is imposed at the entry of the domain (*i.e.* at $x=0$, $\forall z$), that is to say:

$$V_x(x,z)\big|_{x=0} = U_\infty \quad \text{and} \quad V_z(x,z)\big|_{x=0} = 0 \quad \text{for} \quad 0 \leqslant z \leqslant H. \tag{42}$$

At the ordinate $z=0$, between the entry of the domain and the beginning of the plate, the flow is free along the x-axis but maintained purely horizontal for symmetry. There, the boundary conditions are:

$$\left.\frac{\partial V_x(x,z)}{\partial z}\right|_{z=0} = 0 \quad \text{and} \quad V_z(x,z)_{|z=0} = 0 \quad \text{for} \quad 0 < x < (L/5). \tag{43}$$

Our horizontal slotted flat plate is considered as a macroscopic homogeneous permeable medium through the coefficient β_l. Therefore, the boundary conditions on the plate are:

$$\left.\frac{\partial V_x(x,z)}{\partial z}\right|_{z=0} = \beta_l V_x(x,z)_{|z=0} \quad \text{(partial slip condition)} \tag{44}$$

and

$$V_z(x,z)_{|z=0} = 0 \quad \text{(symmetry of the flow in the plane of the plate)} \tag{45}$$

for $(L/5) \leqslant x \leqslant L$.

At the upper limit of the domain (*i.e.* at $z=H$, $\forall x$) and at the end of the channel (*i.e.* at $x=L$, $\forall z>0$), the flow is totally free, therefore:

$$\left.\frac{\partial V_x(x,z)}{\partial z}\right|_{z=H} = \left.\frac{\partial V_z(x,z)}{\partial z}\right|_{z=H} = 0 \tag{46}$$

and

$$\left.\frac{\partial V_x(x,z)}{\partial x}\right|_{x=L} = \left.\frac{\partial V_z(x,z)}{\partial x}\right|_{x=L} = 0. \tag{47}$$

4.2. Numerical method

As in Section 2.2, we are using an iterative procedure to calculate the steady flow. So, the complete two-dimensional Navier–Stokes equations are discretized in time following a first order implicit scheme, linearized and then discretized spatially following the finite volume method on staggered Cartesian meshes. Their resolution is performed on a centred (second order) scheme. The pressure field is calculated on the nodes of the main grid while the two velocity components are determined on two staggered grids. The algorithm that we are using for processing the coupling between the pressure and velocity fields is based on the Augmented Lagrangian technique which corresponds to the implicit processing of the classical artificial compressibility method (Fortin et Glowinski, 1982). This technique leads to a linear coupled system whose unknown quantities are the velocity components $V_x(x,z)$ and $V_z(x,z)$. This linear system is solved by the conjugate gradient method Bi-CGStab preconditioned by an incomplete Gauss factorization.

4.3. Results

The Navier–Stokes equations have been solved on a regular Cartesian mesh of 101 points along the x-axis times 51 points along the z-axis. The length L of the channel was chosen equal to 5 for $Re_l = 100$ and equal to 10 for $Re_l = 1,000$ in order to avoid the boundary layer being too strongly influenced by the boundary condition at the upper limit of the domain.

4.3.1. *Reduced horizontal velocity profiles*

Figures 14 and 15 show the reduced horizontal velocity $V_{hr} = V_x(x,z)/U_\infty$ as a function of the ordinate z for three different values of the abscissa x on the plate (*i.e.* $x = L/5$, $x = 2L/5$ and $x = 3L/5$ on a plate of length $4L/5$) and four of the coefficient β_l and respectively for the two Reynolds numbers $Re_l = 100$ and $Re_l = 1,000$. The Blasius profiles reported as reference have been obtained from the resolution of Equation (17) for a wide range of values of η — each pair (x,z) of coordinates leading to a single value of η — separated by 10^{-4} from their nearest neighbours so as to obtain very precise curves.

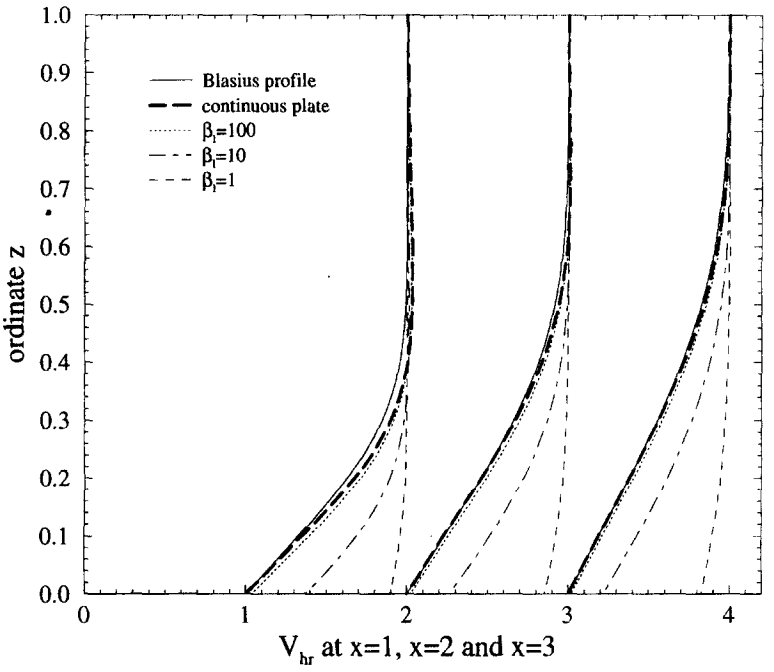

Fig. 14. – Reduced horizontal velocity $V_{hr} = V_x(x,z)/U_\infty$ as a function of the ordinate z for three different values of the abscissa x on the plate and of the coefficient β_l and for the Reynolds number $Re_l = 100$.

First, for $\beta_l \geqslant 10$, we notice a faint excess speed near the leading edge of the plate: there, as the ordinate z increases, the horizontal velocity $V_x(x,z)$ increases beyond U_∞ before decreasing to U_∞ far above the plate. Then, this phenomenon vanishes as the abscissa x on the plate increases. It is not a numerical artifact but the result of two physical considerations. First, the flow is incompressible and the excess speed is a consequence of the flow rate conservation. Second, the singularity that constitutes the leading edge (the thickness of which is not equal to zero but equal to the height of one control volume) modifies the velocity field in a small region after the beginning of the plate, a region where the local form of the Reynolds number $Re_x = (x/l)Re_l$ is small and thus where the viscous effects of the flow are important. This confirms that the Blasius theory, and by extension the modified Blasius formalism, does not apply to low Reynolds numbers.

Below $\beta_l = 10$, the plate is too permeable to disrupt the velocity field so that no excess speed is observed.

We can draw other lessons from Figures 14 and 15. Indeed, they are in accordance with the ones drawn from Figures 6 and 9: the approximation of a continuous plate cannot be made when the slip coefficient is less than $10\sqrt{Re_l}$ since the slip velocity is not negligible at the wall; the boundary layer thickness decreases as the slip coefficient decreases and as the Reynolds number of the flow increases.

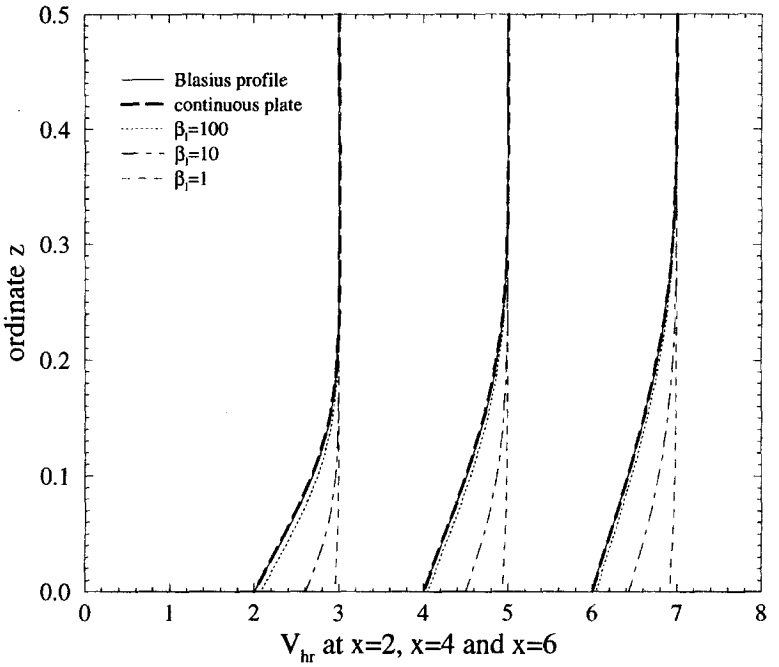

Fig. 15. – Reduced horizontal velocity $V_{hr} = V_x(x,z)/U_\infty$ as a function of the ordinate z for three different values of the abscissa x on the plate and of the coefficient β_l and for the Reynolds number $Re_l = 1,000$.

4.3.2. *Reduced slip velocity along the plate*

Figures 16 and 17 show the reduced slip velocity on the plate $V_p = [V_x(x,z)/U_\infty]_{|z=0}$ as a function of the abscissa x on the plate for different values of the coefficient β_l respectively for $Re_l = 100$ and $Re_l = 1,000$. The "theoretical profiles" have been calculated from Equation (33). They correspond to the asymptotic behaviour pointed out for high values of the coefficient β_l and expressed by Equation (33).

In both figures, we can see that the agreement between the numerical and the theoretical profiles (presented for $\beta_l \geqslant 100$) is quite good for $Re_l = 100$ and really good for $Re_l = 1,000$ beyond $\beta_l = 100$ as soon as we move away from the boundaries of the channel. Actually, at the end of the channel, the difference between the profiles is due to the boundary conditions: in theory, the flow is never totally free far from the leading edge of the plate. At the beginning of the plate, a difference is noticeable too. It has another origin: as explained in Section 3.3, the theoretical profile tends towards a singularity (here $+\infty$) at the leading edge while the numerical result decreases from its original value (equal to 1 in this case since the slip velocity $V_x(x,z)$ is reduced by the velocity at infinite U_∞), before the leading edge.

Logically, due to the invalidity of the modified Blasius formalism for low Reynolds numbers, the distance beyond the leading edge on which a difference between the profiles is observed increases as β_l decreases.

For lower values of the coefficient β_l, we note once again that the reduced slip velocity becomes less affected by the permeable plate as β_l decreases and tends to the asymptotic behaviour expressed by Equation (35). In other words, an extremely porous plate has virtually no effect on the flow.

4.3.3. *Reduced shear stress at the wall*

Figures 18 and 19 show the reduced shear stress at the wall τ_w as a function of the abscissa x on the plate for different values of the coefficient β_l respectively for $Re_l = 100$ and $Re_l = 1,000$. The "theoretical profile"

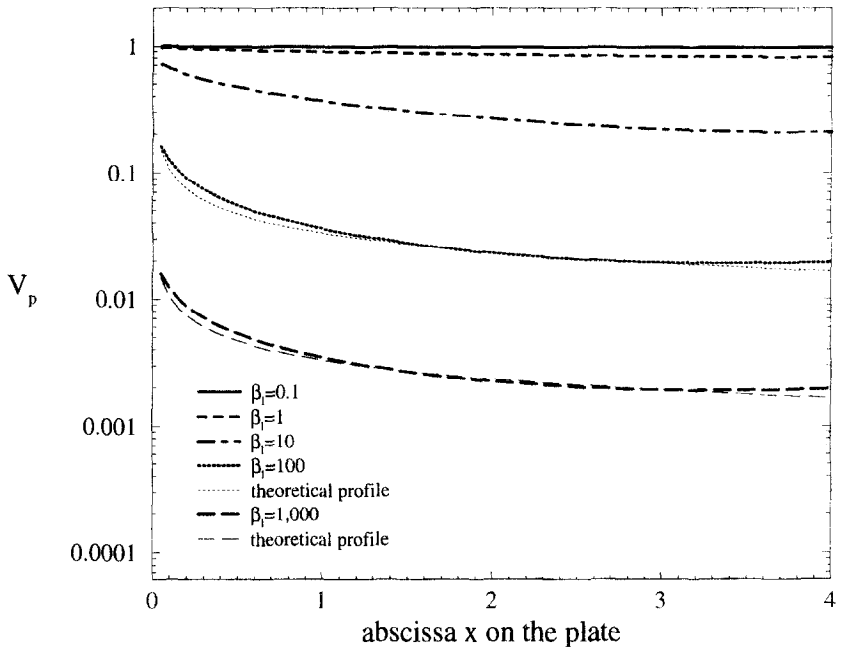

Fig. 16. – Reduced slip velocity along the plate $V_p = [V_x(x,z)/U_\infty]_{z=0}$ as a function of the abscissa x on the plate for different values of the coefficient β_l and for the Reynolds number $Re_l = 100$.

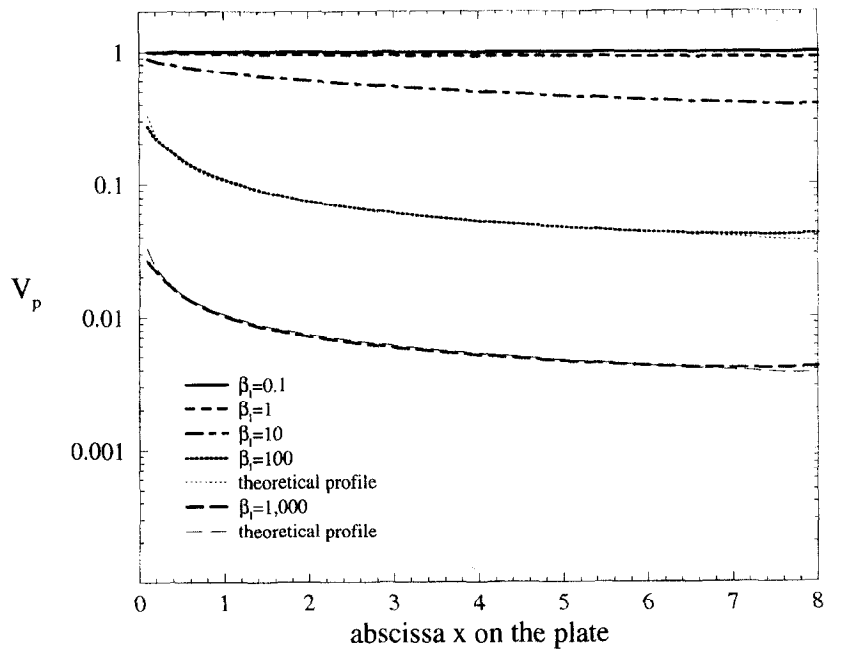

Fig. 17. – Reduced slip velocity along the plate $V_p = [V_x(x,z)/U_\infty]_{z=0}$ as a function of the abscissa x on the plate for different values of the coefficient β_l and for the Reynolds number $Re_l = 1,000$.

has been calculated from Equation (38) which describes the asymptotic behaviour of the shear stress at the wall as the coefficient β_l becomes high.

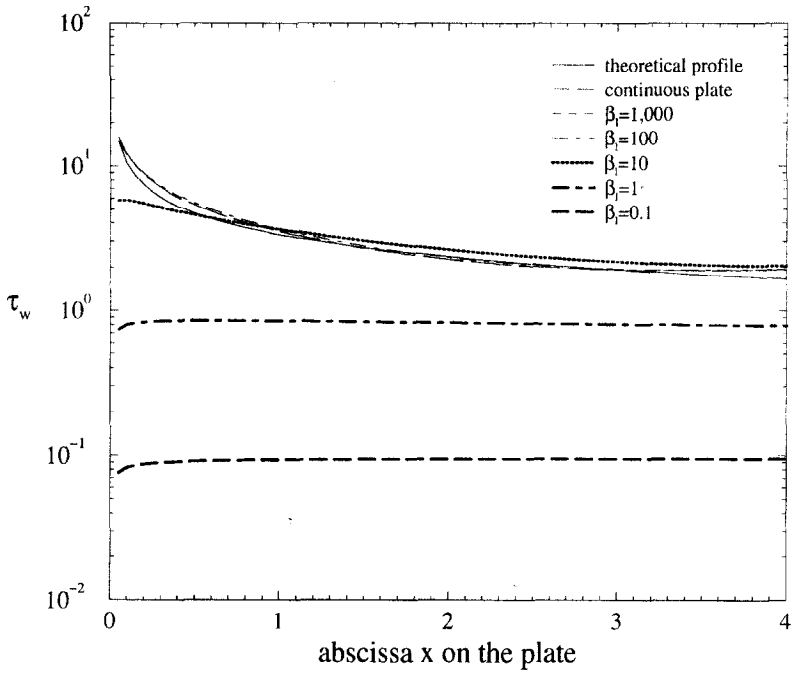

Fig. 18. – Reduced shear stress at the wall τ_w as a function of the abscissa x on the plate for different values of the coefficient β_l and for the Reynolds number $Re_l = 100$.

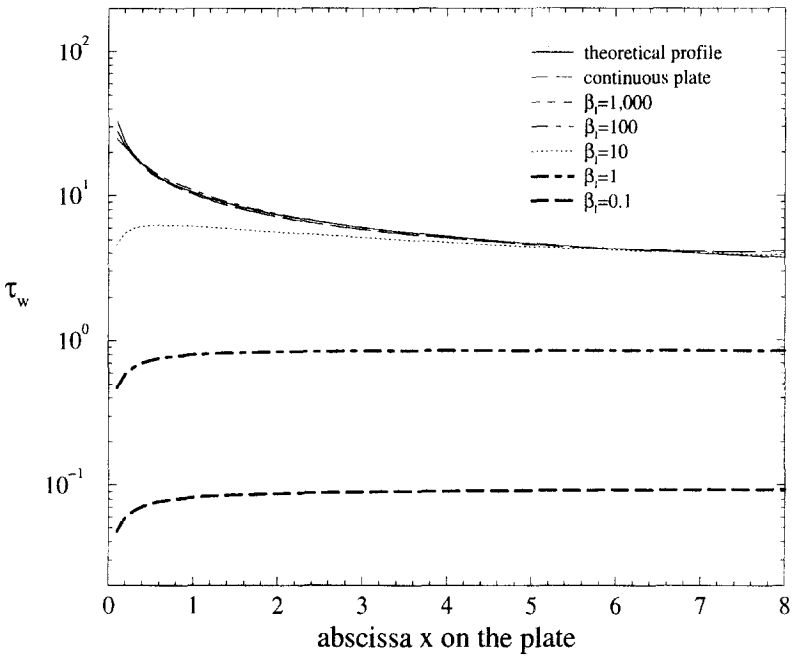

Fig. 19. – Reduced shear stress at the wall τ_w as a function of the abscissa x on the plate for different values of the coefficient β_l and for the Reynolds number $Re_l = 1,000$.

The curves show acceptable accord between the numerical and theoretical profiles beyond $\beta_l \geqslant 10$, except at the end of the channel where the boundary conditions appear to slightly influence the computations. This confirms the validity of Equation (38) for high values of β_l.

On the other hand, as β_l decreases, after a development zone of about an eighth of the length L of the plate (this value is approximate since it seems to depend on the Reynolds number), we observe that τ_w becomes independent of the abscissa x on the plate and of the Reynolds number Re_l of the flow. This fact tends to confirm the asymptotic behaviour expressed by Equation (39).

The real effect of the leading edge of the plate is also interesting to analyse: it appears that, for $\beta_l \leqslant 10$, the shear stress at the wall increases beyond the beginning of the plate before stabilizing to the value of β_l. So, the influence of the leading edge appears beyond the beginning of the plate.

5. Summary

Our study leads us to the following principal conclusions.

First, we have proved that the partial slip boundary condition applies to periodic (at least) slotted or perforated surfaces. The slip coefficient that appears in this condition is strongly correlated with the surface porosity. It increases with the Reynolds number of the flow beyond a certain threshold (that we evaluate) but remains constant below this value. We have also shown that this coefficient tends towards an asymptotic value that corresponds to an isolated plate placed in a purely tangential flow. Thus, we have demonstrated that we could characterize a nearly isolated plate from a study performed on a finite domain.

Afterwards, we have introduced the partial slip boundary condition in the classical Blasius formalism and then studied the boundary layer flow over a zero thickness slotted flat plate, considered as a macroscopic zero thickness homogeneous permeable flat plate. Defining some Reynolds numbers and slip coefficient ranges, we have proposed several formulae that express the reduced boundary layer thickness, the reduced slip velocity on the plate and the reduced shear stress at the wall and their asymptotic behaviour as functions of the slip coefficient, the Reynolds number of the flow and the reduced abscissa on the plate.

Then, we have compared these macroscopic laws to direct numerical simulation results in order to set up the limits of the validity of the modified Blasius formalism. We have proved that this formalism describes, in a very satisfactory way, the evolution of the boundary layer flow over a homogeneous permeable flat plate as soon as the boundary layer theory becomes applicable beyond the leading edge.

The next stage of this study will consist in studying the influence along the plate of periodical succession of solid strips and perforations on the local evolution of the boundary layer, using a two-dimensional direct numerical simulation. Our first results, presented in Laplace (1997), show the role played by the leading edge of the plate and the thickness of the solid strips, together with the Reynolds number of the flow, on the modification of the boundary layer development.

Another way to conclude our work is to check the validity of the partial slip boundary condition on three-dimensional perforated media, which are closer to real configurations than the two-dimensional models we have considered. The parametric study that would follow would allow the results presented in this paper to be corroborated.

REFERENCES

ARQUIS E., CALTAGIRONE J.-P., LE BRETON P., 1991, Détermination des propriétés de dispersion d'un milieu périodique à partir de l'analyse locale des transferts thermiques, *C. R. Acad. Sci. Paris*, **313**, série II, 1087–1092.

BEAVERS G. S., JOSEPH D. D., 1967, Boundary conditions at a naturally permeable wall, *J. Fluid Mech.*, **30**, 197–207.

FENDELL F. E., 1970, On linearized theory for compressible viscous planar flow with slip, *Quart. Appl. Math.*, **28**, 37–55.

FORTIN M., GLOWINSKI R., 1982, Méthodes de Lagrangien Augmenté — application à la résolution numérique de problèmes aux limites, *Méthodes Mathématiques de l'Informatique*, Dunod, Paris, France.

HOCKING L. M., 1976, A moving fluid on a rough surface, *J. Fluid Mech.*, **76**, 801–817.

LAPLACE P., 1997, Approches microscopique et macroscopique des écoulements au voisinage d'une paroi perforée, *Doctoral thesis*, Université Bordeaux I (France).

LAURMANN J. A., 1961, Linearized slip flow past a semi-infinite flat plate, *J. Fluid Mech.*, **11**, 82–96.

MIKSIS M. J., DAVIS S. H., 1994, Slip over rough and coated surfaces, *J. Fluid Mech.*, **273**, 125–139.

PATANKAR S. V., 1980, Numerical Heat Transfer and Fluid Flow, Series in Computational Methods in Mechanics and Thermal Sciences, *Hemisphere Publishing Corporation*, Washington (USA), 131–134.

RICHARDSON S., 1971, A model for the boundary condition of a porous material. Part 2, *J. Fluid Mech.*, **49**, 125–139.

RICHARDSON S., 1973, On the no-slip boundary condition, *J. Fluid Mech.*, **59**, 707–719.

SAFFMAN P. G., 1971, On the boundary condition at the surface of a porous medium, *Stud. Appl. Math.*, **2**, 93–101.

SARKAR K., PROSPERETTI A., 1996, Effective boundary conditions for Stokes flow over a rough surface, *J. Fluid Mech.*, **316**, 223–240.

SCHLICHTING H., 1987, Boundary-Layer Theory, *McGraw-Hill, Inc.*, New York (USA), 127–136.

SHIH T. M., 1984, Numerical Heat Transfer, Series in Computational Methods in Mechanics and Thermal Sciences, *Hemisphere Publishing Corporation*, Washington (USA), 225–230.

TUCK E. O., KOUZOUBOV A., 1995, A laminar roughness boundary condition, *J. Fluid Mech.*, **300**, 59–70.

VAN DER VORST H. A., 1992, Bi-CGStab: A fast and smoothly converging variant of Bi-CG for the solution of non-symmetric linear systems, *SIAM, J. Sci. Stat. Comp.*, **13**, 631–644.

(Manuscript received July 23, 1996;
revised August 15, 1997;
accepted November 3, 1997.)